EFFECTS OF FLUID AND COMPUTED TOMOGRAPHIC TECHNICAL FACTORS ON CONSPICUITY OF CANINE AND FELINE NASAL TURBINATES

RAIMONDA UOSYTE, DARREN J. SHAW, DANIELLE A. GUNN-MOORE, EDUARDO FRAGA-MANTEIGA, TOBIAS SCHWARZ

Turbinate destruction is an important diagnostic criterion in canine and feline nasal computed tomography (CT). However decreased turbinate visibility may also be caused by technical CT settings and nasal fluid. The purpose of this experimental, crossover study was to determine whether fluid reduces conspicuity of canine and feline nasal turbinates in CT and if so, whether CT settings can maximize conspicuity. Three canine and three feline cadaver heads were used. Nasal slabs were CT-scanned before and after submerging them in a water bath; using sequential, helical, and ultrahigh resolution modes; with images in low, medium, and high frequency image reconstruction kernels; and with application of additional posterior fossa optimization and high contrast enhancing filters. Visible turbinate length was measured by a single observer using manual tracing. Nasal density heterogeneity was measured using the standard deviation (SD) of mean nasal density from a region of interest in each nasal cavity. Linear mixed-effect models using the R package '*nlme*', multivariable models and standard *post hoc* Tukey pair-wise comparisons were performed to investigate the effect of several variables (nasal content, scanning mode, image reconstruction kernel, application of post reconstruction filters) on measured visible total turbinate length and SD of mean nasal density. All canine and feline water-filled nasal slabs showed significantly decreased visibility of nasal turbinates ($P < 0.001$). High frequency kernels provided the best turbinate visibility and highest SD of aerated nasal slabs, whereas medium frequency kernels were optimal for water-filled nasal slabs. Scanning mode and filter application had no effect on turbinate visibility.

Key words: artifact, cat, conchae, CT, dog, nose.

Introduction

TURBINATE DESTRUCTION IS AN important diagnostic imaging criterion in the differentiation of aggressive and nonaggressive canine and feline nasal disease.[1–4] Turbinate destruction is commonly associated with malignant nasal neoplasia and fungal rhinitis,[1–3,5–10] whereas turbinates are usually preserved in viral, bacterial, and parasitic canine rhinitis.[4] In cats, this distinction is less clear as viral, bacterial, and lymphoplasmacytic rhinitis can also cause osteolysis of nasal turbinates, albeit usually less marked.[4,11] Computed tomography has been established as a highly sensitive and specific diagnostic imaging test for canine and feline nasal disease[6,9,10,12–14] and nasal turbinate destruction is often easily visible when using the appropriate window settings.[6,15]

However in many dogs and cats with nasal disease the nasal turbinates are surrounded by fluid or soft tissue swelling. This creates an ambiguity over the integrity of the nasal turbinates. We suspect that poor conspicuity of nasal turbinates is not always related to turbinate destruction, and that it can be an artifactual result of neighboring fluid or soft tissue. This has been shown to be the case in nasal radiography[5] but not CT yet.

Technical parameters can have a marked effect on CT image quality.[16] There are some reports investigating the effect of technical parameters on CT image quality in the canine head,[17–19] but none yet for nasal turbinate conspicuity, its relationship with neighboring fluid, nor for the feline head.

From the Royal (Dick) School of Veterinary Studies & The Roslin Institute, The University of Edinburgh, Roslin, Midlothian, Scotland, EH25 9RG, UK.

Portions of this study were presented at the EVDI Annual Scientific Conference, August 30–31, 2011 in London, UK.

Dr. Uosyte's current address is Veterinary Teaching Hospital, The University of Helsinki, Viikintie 49 (P.O. Box 57), 00014 Helsinki, Finland.
Dr. Fraga-Manteiga's current address is Southern Counties Veterinary Specialists, Forest Corner Farm, Hangersley, Ringwood, Hampshire, BH24 3JW, UK.

The copyright line for this article was changed on October 9, 2015 after original online publication.

Address correspondence and reprint requests to Tobias Schwarz at the above address. E-mail: Tobias.Schwarz@ed.ac.uk

Received September 23, 2014; accepted for publication March 7, 2015.
doi: 10.1111/vru.12263

The first aim of our study was to establish whether fluid effaces the nasal turbinates on CT images. We hypothesized that fluid reduces turbinate conspicuity in the canine and feline nasal cavity. The second aim was to determine the optimal imaging protocol that would maximize turbinate conspicuity in aerated and fluid filled nasal cavities. We hypothesized that high frequency kernels would provide the best conspicuity of the nasal turbinates.

Materials and Methods

Freshly dissected cadaver heads of dogs and cats that had been euthanized for clinical reasons, unrelated to nasal disease, were used for this study. Inclusion criteria skeletal maturity, absence of nasal disease or postmortem-related nasal effusion; and being domestic shorthair for cats and of mesaticephalic skull type for dogs. This was verified with an initial CT scan of the entire head reviewed by a board certified veterinary radiologist (T.S.). Animals who did not meet the inclusion criteria were excluded from the study. Canine skull measurements were taken from the topographic CT planning radiograph and the skull index was calculated.[20] A skull index (skull width × 100/skull length) range of 50–60 was used as inclusion criteria for mesaticephalic skull type.[20] The cadaver heads that met the inclusion criteria were then frozen to –80°C and approximately 1-cm thick transverse slabs of nasal cavity were obtained with a bandsaw (600 Series, AEW Delford, Norwich, UK). In the canine cadaver heads two slabs were obtained; one rostral slab includes the 104 to 106 tooth roots and one caudal slab including the 107 and 108 tooth crowns. In the feline cadaver heads only one transverse slab was obtained including the 104 to 107 tooth roots due to the short length of the cat's nose.

Later the sliced nasal slabs were defrosted at 18°C for approximately 10 h. Defrosted nasal slab(s) for each animal were placed in an individual small plastic container (PRUTA, IKEA of Sweden, Älmhult, SE-34381, Sweden) (Fig. 1). For the dog samples, the slabs were positioned in an anatomical orientation with foam between the two slabs. The containers were then scanned with CT. The plastic containers containing the nasal slabs were then filled with room temperature (18°C) water and left for approximately 17 h. This assured maximal water distribution between the nasal turbinates and resulted in edema of the nasal turbinate mucosa. With the water still in place, and the same anatomical orientation set previously, CT scans were then repeated. Nasal slabs that were incompletely filled with fluid and/or contained numerous air bubbles were excluded from the study.

A helical 4-slice CT unit (Somatom Volume Zoom, Siemens, Germany) was used. Constant CT settings included 120-kV tube voltage, 100 to 206-mAs adaptive tube current, 0.5-mm anode focal spot, 1-s tube rotation time, 130-mm display field of view (FOV), 512^2-image matrix, and 1-mm slice width (except for the ultrahigh resolution mode images which were taken with 0.5-mm slice width).

Variable CT settings included sequential, helical, and ultrahigh resolution (UHR) helical modes. All helical series were performed with a detector pitch of 2. The UHR settings included application of special comb-shaped collimators, an ultrahigh frequency image reconstruction kernel, and a slice width of 0.5 mm. With every scanning mode images in low, medium, and high frequency image reconstruction kernels were also reconstructed: with proprietary terms of H30, H31, U40, H40, H41, H50, H70, U70, and U90; H: Head; U: ultrahigh frequency kernel; and the number in the kernel name corresponding roughly to the spatial frequency magnitude of the image reconstruction kernel. After image reconstruction two proprietary filters were also applied to one reconstruction of each mode with the longest measured total turbinate length: posterior fossa optimization (PFO) which reduces beam hardening artifact and high contrast enhancement (HCE) which increases contrast resolution and image sharpness.

After generation of all image series a single slice location on the air-filled and the fluid-filled nasal slab CT series was selected with the anatomical location exactly matching for both series of the same head, and at the same tooth level for all heads of the same species. All assessments and measurements were performed at this slice location using dedicated DICOM viewer software (Osirix, Geneva, Switzerland, version 3.9.2-64bit) on a computer workstation (Apple IMac 27 inch, Apple, USA) with a calibrated monitor. A window width of 4000 Hounsfield units (HU) and a window level of 700 HU were used for all image assessments.

The parameters of the total turbinate length and standard deviation (SD) of the mean nasal density were quantitatively evaluated. Using an open polygon measurement tool of the viewing software, all turbinates were manually traced; their individual lengths were recorded and summated. Turbinates from the left and right nasal cavities of rostral and caudal nasal slabs were summated separately and the nasal septum was excluded (Fig. 2). One round 0.5-cm^2-sized region of interest (ROI) tool from the viewing software was placed in a consistent manner in each nasal cavity for the calculation of the SD of the mean nasal density. In the rostral canine slab and in all feline nasal slabs one ROI was placed in the ventral aspect of the turbinates of each side. In the caudal canine nasal slabs the ROI was centered at the crossing point of horizontal and vertical positioning lines, which emanated from the half-length points of the ventral quadrant lines (Fig. 3). The SD of the mean nasal density calculated by the ROI tool was recorded and used for statistical evaluation.

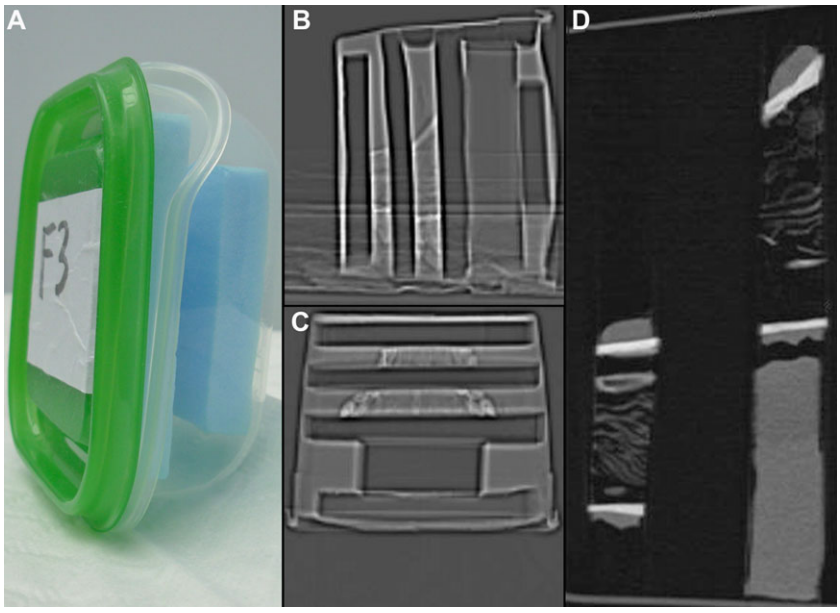

FIG. 1. Plastic container used for the experiment (feline part) containing fitted foam slabs (A). Sagittal and dorsal CT topograms of water filled containers with canine nasal slabs (B, C). Sagittally reconstructed CT image of the container with foam separated canine nasal slabs (D).

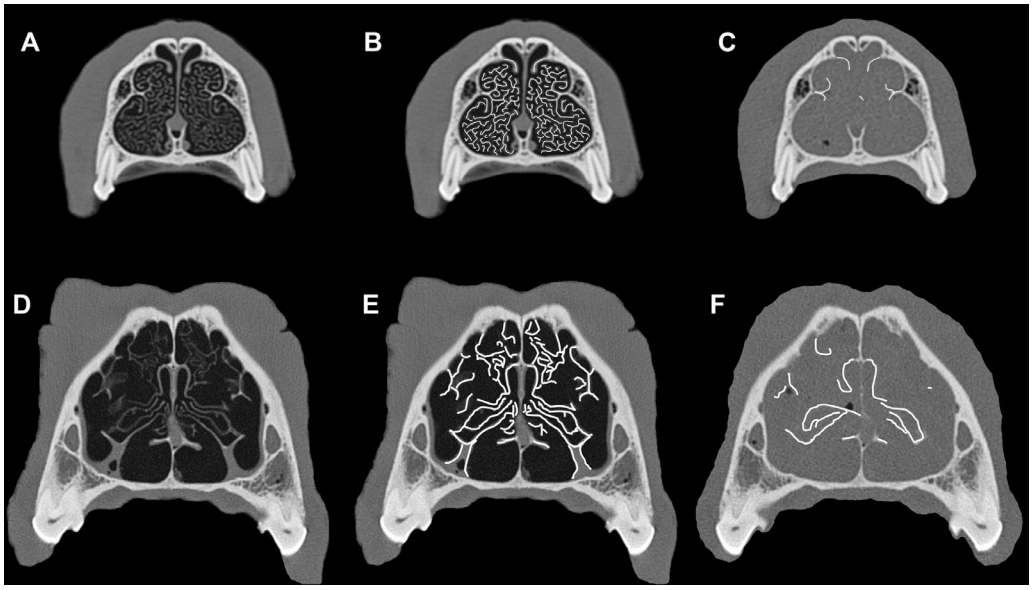

FIG. 2. Transverse CT images of a rostral (A, B, C) canine nasal slab at the level of the 106 tooth and caudal (D, E, F) canine nasal slab at the mesiobuccal and mesiopalatal roots of the 108 tooth. (A, D) Air-filled without tracing; (B, E) air-filled with tracing (white lines) of turbinate length; and (C, F) water-filled with tracing. There is a marked reduction of visible turbinates when they are surrounded by fluid and/or in the presence of turbinate mucosal edema, indicative of effacement.For clarity these images were edited with software (Adobe Photoshop CS5, version 12.01, Adobe Systems Inc., San Francisco, CA) including cropping, application of tracer lines, and removal of extranasal water background.

Statistical Methods

Statistical analysis was performed by the first and the second authors. All calculations were carried out using commercial software (R v3.0.0, © The R Foundation for Statistical Computing 2013) to investigate the effect of several variables (nasal content, scanning mode, image reconstruction kernel, and application of post reconstruction filters) on measured visible total turbinate length and the SD of the mean nasal density. The analysis was performed separately for each species. The data sets required log transformation before analysis in order that the residuals were normally distributed. Linear mixed-effect models using the R package '*nlme*' were carried out in order that the multiple measurements that were obtained from each cadaver could be entered as a random effect.[21] Kernels (from

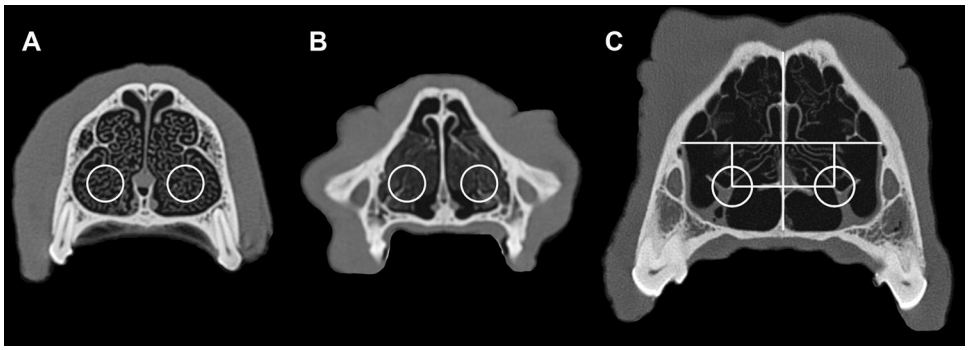

FIG. 3. Transverse CT images of air-filled canine and feline nasal slabs demonstrating placement of 0.5-cm^2-sized regions of interest (ROI) for the calculation of standard deviation of mean density. (A) A rostral canine nasal slab image at the level of the mesial root of the 106 tooth, (B) a feline nasal slab image at the level of the mesial root of the 107 tooth and (C) a caudal canine nasal slab image at the level of the mesiobuccal and mesiopalatal roots of the 108 tooth. The ROIs were placed in the ventral aspect of each nasal cavity in (A) and (B). In the caudal canine nasal slab image (C) the ROI was centered at the crossing point of horizontal and vertical positioning lines which emanate from the half-length points of the ventral quadrant lines.

standard and high resolution H30, H31, U40, H41, H50, H70, U70 and U90) were re-entered as fixed effects into separate models. Multivariable models were later performed on the standard resolution (H30, H31, H40, H41, H50, and H70) data looking at differences between modes and filters once the kernel which gave the longest length had been selected. For all the canine analyses whether measurements were caudal or rostral was taken into account by adding slab location as a confounder prior to adding any of the other fixed effects. The results reported for canine data are therefore differences between groups (kernels, etc) having first accounted for the differences observed with slab location. Differences within kernels and filters were investigated using standard *post hoc* Tukey pair-wise comparisons using the '*multcomp*' package (v1.2–17). Statistical significance was taken at $P < 0.05$.

Results

Three canine and three feline cadaver heads met the inclusion criteria for the study. A rostral nasal slab image at the level of the 106 tooth and a caudal nasal slab image at the level of the 108 tooth were used for each canine head and a nasal slab image at the level of the 107 tooth was used for each feline head. It was possible to trace turbinates in all images.

Turbinate Length

The mean total nasal turbinate length of all canine heads measured in the caudal slab was significantly longer than in the rostral slab ($P < 0.001$), so slab location was taken into account for all remaining analyses in dogs. The mean total nasal turbinate length of all canine and feline heads was significantly longer in air-filled nasal slabs compared to water-filled nasal slabs ($P < 0.001$, Figs. 4A and 5A). There were also significant differences in the mean total nasal turbinate length between different image reconstruction kernels within both the water- and the air-filled subgroups ($P < 0.001$, Figs. 4B and 5B) in both species.

In dogs, despite the relatively small differences observed between kernels (mean difference [Δ_m] < 4.51 cm), the H70 kernel provided a longer turbinate length compared to the other kernels in air-filled slabs ($\Delta_m > 1.93$ cm, $P < 0.001$, Fig. 4B), with the H50 kernel also having a longer length than H30, H31, and H40 kernels ($\Delta_m > 1.37$ cm, $P < 0.042$). However, the only difference observed in the water-filled nasal slabs was a significantly longer turbinate length with H50 compared to H31, H41, and H70 kernels ($\Delta_m > 0.62$ cm, $P < 0.039$).

In cats, the high frequency kernels H50 and H70 significantly increased the mean total nasal turbinate length in both air- and water-filled slabs compared to applying other kernels ($P < 0.001$, Fig. 5B). Applying the highest frequency image reconstruction kernel for the standard mode head protocols with the H70 kernel also significantly increased the turbinate length compared to H50 in air-filled ($P < 0.001$), but not water-filled slabs ($\Delta_m = 0.73$ cm, $P = 0.621$).

Filter application to the image series in which the longest total nasal turbinate length resulting kernel (H70) was used made no significant difference to mean total nasal turbinate length in either air- or water-filled nasal slabs in dogs ($P > 0.104$, Fig. 4C) or cats ($P > 0.272$, Fig. 5C).

In dogs, no difference in total turbinate length was observed in air-filled nasal slabs with H70 kernels in helical mode compared to sequential mode ($P = 0.725$, Fig. 4D), whereas in cats there was a small increase in turbinate length in helical mode ($\Delta_m = 1.15$ cm, $P = 0.012$, Fig. 5D). In water-filled nasal slabs the total turbinate length observed in helical mode with an H50 kernel was longer than in the equivalent sequential mode in dogs ($\Delta_m = 1.87$ cm, $P < 0.001$, Fig. 4D), but not in cats ($\Delta_m = 0.3$ cm, $P = 0.378$, Fig. 5D).

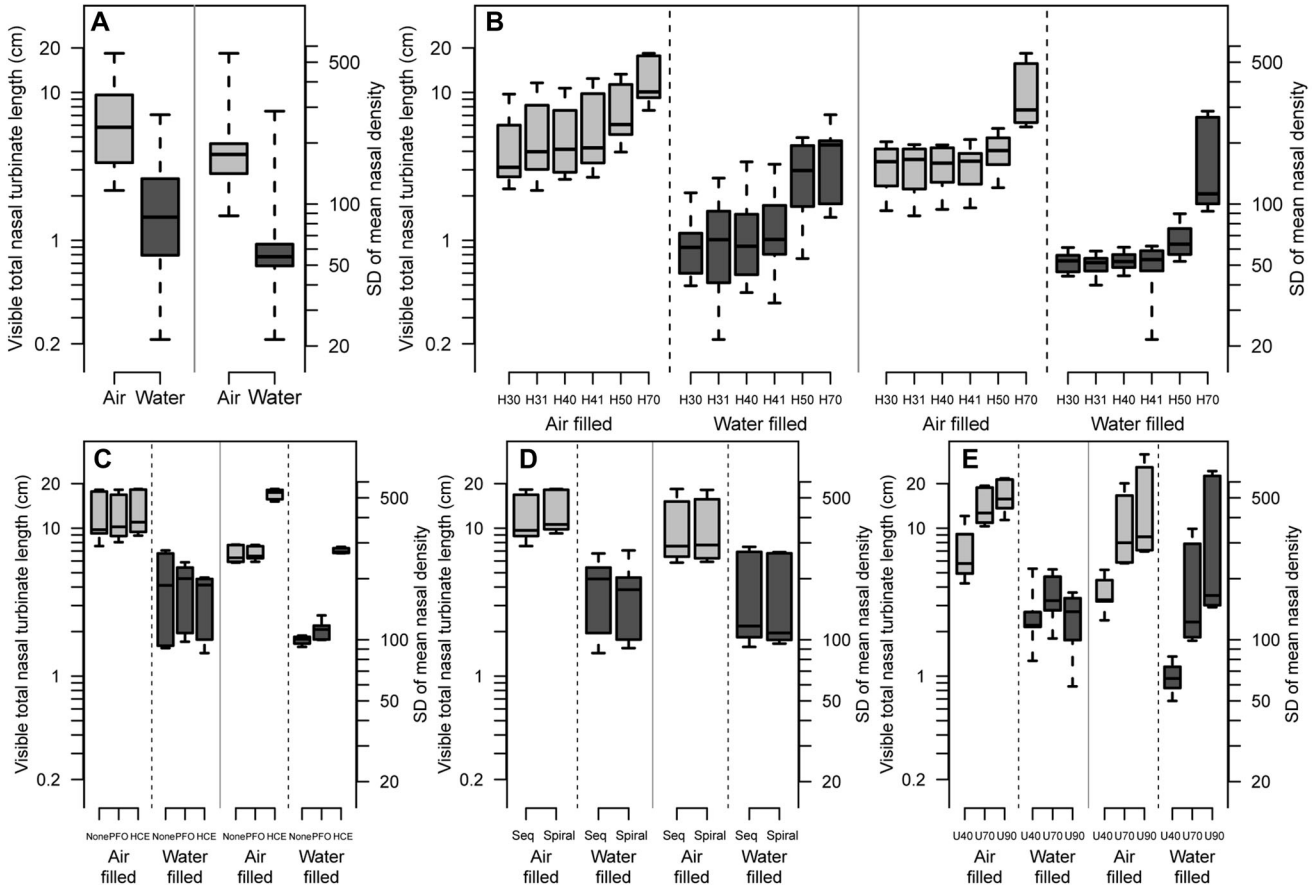

FIG. 4. Boxplots representing the $\log_{10}$ transformed total length of nasal turbinate length visibility and the $\log_{10}$ transformed standard deviation of mean nasal density in canine nasal slabs subdivided into whether air- or water-filled: (A) overall; (B) sub-divided by kernel (H30, 31, 40, 41, 50, 70); (C) subdivided H70 kernel by filter, subdivided H50 kernel by filter in water filled; (D) subdivided H70 kernel by mode, subdivided H50 kernel by mode; and (E) total length by kernel (U40, U70, U90) in high resolution mode. For all plots both caudal and rostral slab data are included and the horizontal line in each box delineates the median value, the shaded boxes the interquartile range and the whiskers the full data range. PFO: posterior fossa optimization image filter, HCE: high contrast enhancement filter.

If only the kernels from the UHR mode were considered (U40, U70, and U90, Figs. 4E and 5E), U70 and U90 kernels resulted in significantly longer total turbinate length than the U40 kernel in air-filled nasal slabs in dogs ($\Delta_m >$ 2.92 cm, $P < 0.032$) and cats ($\Delta_m > 6.96$ cm, $P < 0.012$), but shorter lengths in water-filled nasal slabs in dogs ($\Delta_m <$ -0.98 cm) and minimally shorter in cats ($\Delta_m = 1.1$ cm, $P = 0.036$, Fig. 5E).

A comparison between the standard and the UHR helical series with the kernel resulting in the highest mean turbinate length was made to determine the optimal mode and kernel combination. The helical H70 series was compared to the helical UHR U90 series in air-filled canine nasal slabs and all feline nasal slabs and the helical H50 series with the helical UHR U40 series in canine water-filled nasal slabs. In air-filled nasal slab data no difference was observed in dogs ($\Delta_m = 0.22$ cm, $P = 0.599$) whereas in cats the helical UHR U90 series gave the longest turbinate length ($\Delta_m = 3.66$ cm, $P < 0.001$). In water-filled nasal slabs, a longer turbinate length was achieved with the helical H50 series in dogs ($\Delta_m = 2.04$ cm, $P = 0.020$, Fig. 4B and E) and with the helical H70 series in cats ($\Delta_m = 0.93$ cm, $P = 0.010$, Fig. 5B and E), compared to the helical UHR U40.

Standard Deviation

The mean SD of all canine nasal areas measured in the caudal slab was significantly higher ($\Delta_{SD} = 138$) than in the rostral one ($P < 0.001$), and therefore slab location was taken into account for all the remaining analyses.

Air-filled nasal slabs had a significantly wider variation in nasal density, and therefore a higher SD compared to water-filled nasal slabs in dogs ($\Delta_{SD} = 98.8$, $P < 0.001$, Fig. 4A) and cats (SD = 72, $P < 0.001$, Fig. 5A).

Breaking down the SD data by applied kernel revealed overall differences between kernels in both air- and water-filled nasal slabs ($P < 0.001$, Figs. 4B and 5B). The H70

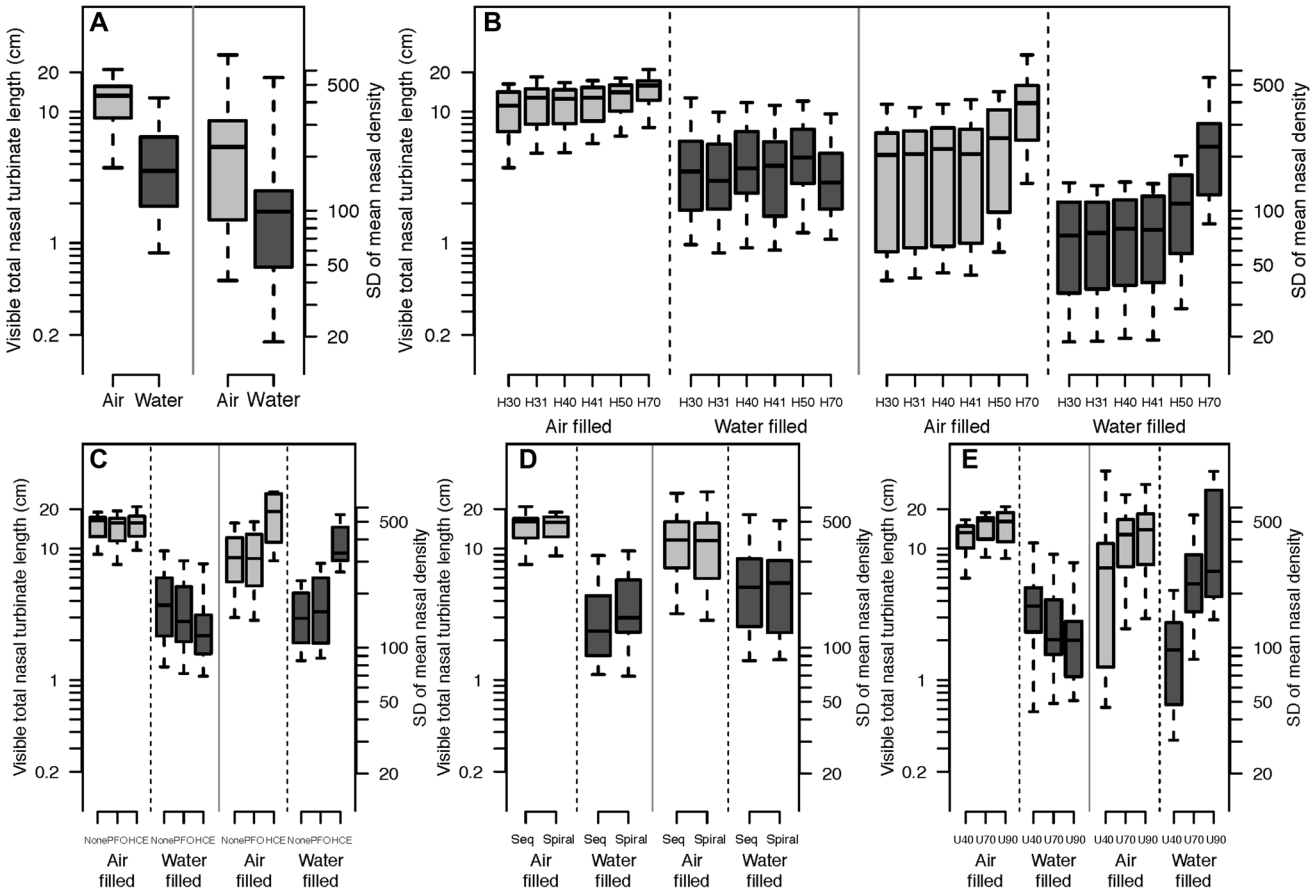

FIG. 5. Boxplots representing the $\log_{10}$ transformed total length of nasal turbinate length visibility and the $\log_{10}$ transformed standard deviation of mean nasal density in feline nasal slabs subdivided into whether air- or water-filled: (A) overall; (B) sub-divided by kernel (H30, 31, 40, 41, 50, 70); (C) subdivided H70 kernel by filter; (D) subdivided H70 kernel by mode; and (E) total length by kernel (U40, U70, U90) in high resolution mode. For all plots the horizontal line in each box delineates the median value, the shaded boxes the interquartile range and the whiskers the full data range. PFO: posterior fossa optimization image filter, HCE: high contrast enhancement filter.

always gave the significantly greatest SD in dogs ($\Delta_{SD} > 113$, $P < 0.001$) and cats ($\Delta_{SD} > 79.9$, $P < 0.001$).

The HCE filter application to the H70 kernel data in both air- and water-filled nasal slabs was associated with higher SD compared to either no filter or a PFO filter in dogs ($\Delta_{SD} > 205$, $P < 0.001$, Fig. 4C) and cats ($\Delta_{SD} > 162$, $P < 0.001$, Fig. 5C). However, no differences were observed in the SD magnitude between sequential or helical mode with a H70 kernel in either air- or water-filled nasal slabs in dogs ($\Delta_{SD} < 4.3$, $P > 0.912$, Fig. 4D) or cats ($\Delta_{SD} < 5.2$, $P > 0.878$, Fig. 5D).

If only the kernels from the HR mode were considered (U40, U70, and U90), then there was a significant difference in SD between U40 and the other two kernels, irrespective of whether air- or water-filled nasal slabs in dogs ($\Delta_{SD} > 130$, $P < 0.001$, Fig. 4E) and cats ($\Delta_{SD} > 94$, $P < 0.001$, Fig. 5E), but there was no difference between U70 and U90 in any feline nasal slab ($P > 0.163$) or air-filled canine nasal slabs ($\Delta_{SD} = 42.6$, $P = 0.743$). The U90 kernel gave a minimally greater SD compared to the U70 kernel in water-filled canine nasal slabs ($\Delta_{SD} = 114$, $P = 0.049$).

No significant differences were observed in the SD between helical H70 and helical UHR U90 series for air-filled canine nasal slabs ($\Delta_{SD} = 47.7$, $P = 0.326$, Fig. 4B and E) or any feline nasal slabs ($P > 0.073$, Fig. 5B and E). In water-filled canine nasal slabs helical UHR U90 settings resulted in greater SD values than with helical H70 settings ($\Delta_{SD} = 127$, $P = 0.027$, Fig. 4B and E).

Discussion

The results of our study confirm our hypothesis that the conspicuity of canine and feline nasal turbinates is decreased by fluid and mucosal edema on CT images. Conspicuity is the property of being readily visible. Nasal pathologies are frequently associated with increased nasal secretion, inflammatory excretions and/or mucosal edema. Therefore our experimental findings are relevant for

clinical nasal disease, where ubiquitous nasal fluid may mask turbinate bone. Similar findings have been made in an experimental nasal radiography study[5] and have been taken into consideration in clinical canine nasal radiography studies.[1–3,6–10] In radiography, a two-dimensional image is created from a three-dimensional object. The radiographic opacity is the sum of all superimposed opacities of the object (*summation effect*). Borders of adjacent structures of similar opacity will become indistinct, known as the *effacement effect* (synonyms *silhouetting, border obliteration*). Turbinates are paper-thin bone structures and if surrounded by large amount of fluid or soft tissue (e.g. edema), the combination of summation and effacement explains their visual disappearance in radiography. However, CT is a cross-sectional imaging modality, which is superior to radiography due to its far larger range of detectable densities and the almost complete lack of object superimposition in the generation of an image. Therefore, the loss of turbinate conspicuity due to surrounding fluid is unexpected in CT, has not been taken into consideration in clinical nasal CT studies and is likely different from radiography. Opacities are not summated in CT, however there is some density averaging in the creation of a CT image. It occurs within the two planes (z and x–y) of each voxel from which the CT image is generated. Z-plane density averaging corresponds to the selected slice width and x–y plane averaging corresponds to the combination of FOV and image matrix size. In the current study both parameters were chosen to create minimal voxel dimensions (x and y: 0.26 mm; z: 0.5 or 1 mm). Due to the intrinsic spatial resolution limits of the CT scanner it is unlikely that a smaller FOV would have resulted in a higher spatial resolution. With most turbinates being oriented perpendicular to the transverse CT image plane, there should be only limited density averaging of bone with the other structures in the z-plane. In dogs and cats, the normally air-filled 'gap space' between turbinates is on average 0.45 mm and 0.4 mm respectively, exceeding the x–y plane dimension of the voxel.[22] Therefore, density averaging between the turbinates and the gap space in the x–y plane should also be relatively limited. It is likely that additional technical parameters are involved in this process such as point spread function. It defines how a point is spread out in space by the imaging process. No imaging system is ever 100% faithful in depicting the imaged object. The margins of the imaged object are always somewhat blurred and the degree of blur is determined by several factors; one of them is object contrast. With low object contrast, the denser of two neighboring objects usually appear artificially thicker.[23] One CT study demonstrated this by filling canine tympanic bullae with fluid and thereby increasing the apparent bulla wall thickness.[24] However, in the current study bone dense turbinates disappeared when surrounded by less dense fluid and edematous mucosa. We speculate that if the denser structure is very thin and is surrounded by much thicker lower density objects on both sides, the effect is reversed, and soft tissue effacement of the denser structure occurs.

In the current study canine nasal turbinates were better visualized caudally than rostrally. This is most likely related to the anatomy of the nasal turbinates. The ethmoturbinates occupy the most caudal part of the nasal cavity. The dorsal nasal concha arises from the ethmoid crest whereas the ventral nasal concha arises from the conchal crest of the maxilla.[20] The caudal part of the nose contains more turbinate structures and thicker and denser turbinates.[25]

Our second hypothesis that high frequency image reconstruction kernels maximize turbinate conspicuity was partially confirmed by the results of our study. An image reconstruction algorithm or kernel is a mathematical method used to create a matrix image from projectional raw data via Fourier transformation or iterative reconstruction.[16] The exact formulas of CT kernels are closely guarded trade secrets, but the basic common principle is that they are based on the spatial frequency of data sampling and edge performance (sharpening or smoothing of edges). The magnitude of the kernel number roughly corresponds to the magnitude of spatial frequency (Siemens, Toshiba) whereas in other systems the kernels have designated names (General Electrics soft: low, detail: medium, bone: high, edge: very high spatial frequency) or letters (Philips). High spatial frequency kernels (corresponding to higher kernel numbers in the used system in this study) increase image sharpness at the expense of increased image noise.[23] Images should be viewed with a wide display window as done in this study to decrease the visibility of image noise.[16] These kernels are optimal for anatomical regions with wide inherent object contrast latitude such as the aerated nose, and as hypothesized high frequency kernels resulted in the highest turbinate conspicuity in this environment. However our hypothesis was not confirmed for fluid-filled nasal slabs where medium frequency kernels provided maximal turbinate conspicuity. Most likely the reduced object contrast latitude favors such kernels due to their slightly higher contrast resolution. In addition, the point spread function is widest (making dense structures appear thicker) with a lower frequency kernel.[23,26] Not surprisingly, the medium frequency kernel H50 provided maximum turbinate visibility in water-filled canine nasal slabs and was equal in performance with a higher frequency kernel in feline water-filled nasal slabs. An imaging series with a medium and high frequency kernel is therefore recommended for any optimized nasal CT protocol.

The UHR settings in the CT unit used consisted of a combination of very thin slice width, use of special comb shaped collimators, and ultrahigh spatial frequency kernels. The study design did not allow elucidation of how each of these technical parameters contributed to the

imaging performance separately, but it was interesting to note that comparing the different frequency kernels within UHR mode the same tendencies occurred as in standard mode imaging. Comparing the highest scoring UHR and standard mode kernels, the UHR settings appear optimal for aerated small anatomic objects like the feline nose, and are equal in performance to standard settings in the slightly larger canine nose. If fluid- or soft-tissue-pathology is present, standard settings provide more anatomical information. Therefore, in most situations, a standard resolution CT protocol is sufficient for investigation of canine and feline disease, but UHR setting may be beneficial as an additional series for small aerated nasal structures.

Helical mode images provided equal or slightly more anatomic detail than sequential CT images. Most likely this is due to the low pitch used, which may have been sufficiently low to prevent image degradation yet high enough to increase turbinate conspicuity in some cases via data averaging along the *Z*-axis in nasal areas where there is more bone than airspace present. For nasal imaging a helical scan mode is generally preferable for reasons of acquisition speed and quality of orthogonal reconstructions. Helical mode imaging can therefore be recommended for an optimized nasal CT protocol.

Posterior fossa optimization and HCE filters are proprietary retrospective techniques applied to DICOM images (not raw data) in the system used, reducing beam hardening artifacts and increasing image sharpness respectively. Application of these filters made no difference to turbinate visibility in this study. Therefore, they are not beneficial for nasal imaging but are also not harmful and may be applied as appropriate to reduce beam hardening artifacts or increase image sharpness in other areas of the head that may be included in the same imaging series.[18]

The SD of mean tissue density is an objective measure of tissue homogeneity or heterogeneity. It can be used to assess CT artifact magnitude in homogeneous tissue like the brain.[27,28] In this study it was used as an objective measure of density heterogeneity of the canine and feline nose, consisting of bone, soft tissue, and air. This was to complement the part of the study that involved the manual tracing of turbinate length where human vision and perception were potential observer-related biases, thus avoiding Mach lines and other phenomena. The SD results closely matched the results from the turbinate length measuring part of the study, with higher density heterogeneity in aerated compared to fluid-filled nasal slabs and also higher density heterogeneity with a high frequency kernel compared to lower kernels in air-filled nasal slabs. This is supportive of the effacement effect being mainly caused by technical factors of the imaging process, rather than visual and perception effects. However, trends were slightly different in water-filled nasal slabs and with the use of the UHR imaging protocol and application of an HCR filter. We suspect that some of the density differences measured with SD were insufficient to be seen by the human eye or appreciated by the investigators.

This study has several limitations. Due to the large amount of data generated we limited our study to three dogs and three cats. Dogs with a wide variety of skull shapes may have quite diverse turbinate anatomy and our results may not be representative for the entire spectrum. Our study was only performed on one CT unit. Whilst most technical parameters, such as voltage, current, tube rotation time, display FOV, slice width, and helical pitch can be selected identical on any modern CT unit, some are specific to a model or manufacturer such as the image reconstruction kernels and the UHR mode. By investigating a range of kernels we believe we have demonstrated tendencies that should be transferable to different CT models and manufacturers. Using the UHR mode, the influence of the individual technical settings in this mode could not be assessed. However, since similar settings are incorporated in a number of CT units we wanted to assess whether they are useful for nasal CT. Kernels and filters are trade secrets and cannot be directly compared between different CT manufacturers. We did not investigate the influence of slice width and FOV size and chose both parameters as minimal. For many other head structures that are simultaneously assessed on a nasal CT scan, keeping these parameters small is essential[16,19] and therefore would be used in a typical clinical setting. Since we suspect that both slice width and FOV size have some influence on turbinate visibility it would be interesting to investigate this in future studies. We also did not investigate the influence of different display window settings. For the detection of small bone structures such as turbinates a wide window width and a window level at the bone density level is necessary, consistent with our windowing choice. Window optimization has been shown to be very important in the assessment of other structures of the canine head, such as the pituitary gland,[17] and is likely to influence turbinate visibility. This was beyond the scope of this study but would also warrant further investigations. Due to the nature of this study it was not possible to investigate the effect of intravenous contrast medium administration onto turbinate visibility. Based on our experience with clinical cases undergoing a nasal CT examination, the mucosa frequently shows contrast enhancement as a thin linear rim. This can be very helpful to identify the turbinate structures and differentiate mass lesions from secretions. A contrast enhanced CT series should therefore be an integral part of the nasal CT protocol.

In conclusion, neighboring fluid and/or mucosal edema significantly reduces canine and feline nasal turbinate conspicuity in CT. Therefore, in the presence of nasal fluid,

poorly or not visible canine and feline nasal turbinates in CT do not necessarily indicate aggressive osteolytic nasal pathology. Other imaging findings should be corroborated to assess the aggressiveness of nasal disease. An optimized imaging protocol for the canine and feline nose should include a medium- and a high-frequency kernel. If UHR settings are available, then these are most likely beneficial for small patients with aerated nasal cavities.

REFERENCES

1. Gibbs C, Lane JG, Denny JH. Radiologic features of intra-nasal lesions in the dog: a review of 100 cases. J Small Anim Pract 1979;20: 515–535.
2. Sullivan M, Lee R, Skae CA. The radiologic features of sixty cases of intra-nasal neoplasia in the dog. J Small Anim Pract 1987;28:575–586.
3. Sullivan M, Lee R, Jakovljevic S, Sharp NJH. The radiological features of aspergillosis of the nasal cavity and frontal sinuses in the dog. J Small Anim Pract 1986;27:167–180.
4. Suter P. Diseases of the nasal passages and paranasal sinuses. In: Suter P. Thoracic radiography. A text atlas of thoracic diseases of the dog and cat. Wettswil: PF Suter, 1984;206–224.
5. Schmidt M, Voorhout G. Radiography of the canine nasal cavity: significance of the presence or absence of the trabecular pattern. Vet Radiol Ultrasound 1992;33:83–86.
6. Schwarz T. The role of conventional radiography and computed tomography (cat-scan) in the diagnostic of clinical rhinitis in dogs with specific consideration of nasal tumours and fungal rhinitis. Berlin: Veterinary Thesis, Egelsbach-Frankfurt-St.PeterPort: Haensel-Hohenhausen, German Academic Writings Vol. 2418, 1997.
7. Henderson SM, Bradley K, Day MJ, Tasker S, Caney SMA, Hotston Moore A, Gruffydd-Jones TJ. Investigation of nasal disease in the cat – a retrospective study of 77 cases. J Feline Med Surg 2004;6:245–257.
8. Burk RL. Computed tomographic imaging of nasal disease in 100 dogs. Vet Radiol Ultrasound 1992;33:177–180.
9. Karnik K, Reichle JK, Fischetti AJ, Goggin JM. Computed tomographic findings of fungal rhinitis and sinusitis in the cat. Vet Radiol Ultrasound 2009;50:65–68.
10. Tromblee TC, Jones JC, Etue AE, Forrester SD. Association between clinical characteristics, computed tomography characteristics, and histologic diagnosis for cats with sinonasal disease. Vet Radiol Ultrasound 2006;47: 241–248.
11. Schoenborn WC, Wisner ER, Kass PP, Dale M. Retrospective assessment of computed tomographic imaging of feline sinonasal disease in 62 cats. Vet Radiol Ultrasound 2003;44:185–189.
12. Lefebvre J, Kuehn NF, Wortinger A. Computed tomography as an aid in the diagnosis of chronic nasal disease in dogs. J Small Anim Pract 2005;46:280–285.
13. Saunders JH, VanBree H, Gielen I, DeRooster H. Diagnostic value of computed tomography in dogs with chronic nasal disease. Vet Radiol Ultrasound 2003;44:409–413.
14. Drees R, Forrest LJ, Chappell R. Comparison of computed tomography and magnetic resonance imaging for the evaluation of canine intranasal neoplasia. J Small Anim Pract 2009;50:334–340.
15. Saunders J. Chapter 11 – Nasal cavities and frontal sinuses. In: Schwarz T, Saunders J. (eds): Veterinary computed tomography. Oxford: Wiley-Blackwell, 2011;93–110.
16. Schwarz T, O'Brien R. Chapter 2 – CT acquisition principles. In: Schwarz T, Saunders J. (eds): Veterinary computed tomography. Oxford: Wiley-Blackwell, 2011;9–27.
17. Auriemma E, Voorhout G, Barthez PY. Determination of optimal window width and level for measurement of the canine pituitary gland height on computed tomographic images using a phantom. Vet Radiol Ultrasound 2007;48:113–117.
18. Zarelli M, Schwarz T, Puggioni A, Pinilla M, O'Doherty JV, McAllister H. An optimized protocol for multislice computed tomographic of the canine brain. Vet Radiol Ultrasound 2014;55:387–392.
19. Esmans CM, Soukup WJ, Schwarz T. Optimized canine dental computed tomographic protocol in medium-sized mesaticephalic dogs. Vet Radiol Ultrasound 2014;55:506–510.
20. Evans HE. The skull. In Evans HE (ed): Miller's anatomy of the dog. 3rd ed. Philadelphia: Saunders, 1993:128–166.
21. Pinheiro JC, Bates DM. Mixed-effects models in S and S-PLUS. 2nd ed., New York: Springer, 2009.
22. Schroter RC, Watkins NV. Respiratory heat exchange in mammals. Respir Physiol 1989;78:357–368.
23. Joseph P. Artifacts in computed tomography. In: Newton T, Potts D (eds): Radiology of the skull and brain. St. Louis: Mosby, 1981;3956–3992.
24. Barthez PY. Apparent wall thickening in fluid filled versus air filled tympanic bulla in computed tomography. Vet Radiol Ultrasound 1996;37: 95–98.
25. Van Valkenburgh B, Theodor J, Friscia A, Pollack A, Rowe T. Respiratory turbinates of canids and felids: a quantitative comparison. J Zool Lond 2004;264:281–293.
26. Schwarz T. Chapter 4 – Artifacts. In: Schwarz T, Saunders J. (eds): Veterinary computed tomography. Oxford: Wiley-Blackwell, 2011;35–55.
27. Rozeik C, Kotterer O, Preiss J, et al. Cranial CT artifacts and gantry angulation. J Comput Assist Tomogr 1991;15:381–386.
28. Porat-Mosenco Y, Schwarz T, Kass PH. Thick-section reformatting of thinly collimated computed tomography for reduction of skull-base-related artifacts in dogs and horses. Vet Radiol Ultrasound 2004;45:131–135.